1 Megawatt, 20 kHz, Isolated, Bidirectional 12kV to 1.2kV DC-DC Converter for Renewable Energy Applications

G. Ortiz, J. Biela, D. Bortis and J. W. Kolar
Power Electronic Systems Laboratory, ETH Zurich
ETL I16, Physikstrasse 3
CH-8092 Zurich, Switzerland
Email: ortiz@lem.ee.ethz.ch

***Abstract*—The design of a 1 MW, 20 kHz, isolated, bidirectional 12kV to 1.2kV DC-DC converter for renewable energy applications is presented. The main topics addressed are: High-Voltage (HV) side switch, topology & modulation and Medium Frequency (MF) transformer. A study of the possible HV side switches, considering 4.5 kV IGBTs is performed, fixing the requirements from the topology and modulation side in order to reach a highly efficient system. The studied topologies are the Dual Active Bridge (DAB) with triangular modulation and the Series Resonant Converter (SRC) with constant frequency operation. Both topologies are able to achieve Zero Current Switching (ZCS) in the HV side switches, reducing the switching losses in these devices, which contribute to a large share to the system losses. Efficiency curves are presented for different semiconductor technologies for the Low-Voltage (LV) side switch in order to study the trade-offs between the selected topologies. Three MF transformer concepts, namely core-type, shell-type and matrix transformer, are presented and compared in respect of winding arrangement, isolation mechanisms and thermal management. Power losses and volume are calculated in each case and used to compare the different transformer concepts.**

I. Introduction

Problems associated with power generation through limited and CO_2 emitting energy sources are planed to be overcome using renewable energy sources. A study of the European Renewable Energy Council projects that generation through renewable energy will quadruple its contribution to power generation by 2050 [1].

Amongst today's renewable energy sources, wind power generation is currently the main contributor and is being continuously developed further. This trend will increase the current wind turbine power ratings and will further encourage the location of wind farms in shallow seas, as the offshore power generation is projected to considerably increase within the next decades [1, 2]. The offshore installation of these new higher power wind farms introduces new challenges in power transmission and connection to onshore AC transmission/distribution grids. Research has shown that High Voltage Direct Current (HVDC) power transmission suits better the requirements of medium/large distance, e.g. 100/200km, power transmission in relation to classical AC transmission lines because no reactive power is produced/consumed by the transmission cable, reducing the losses in the power transmission system [3].

One of the proposed [2, 4] future wind farm DC layouts is shown in Fig. 1-a) as an example. Here, several wind turbines with DC output are connected in series to reach the HVDC transmission level, avoiding the installation of an offshore HVDC station. Groups of these series connected wind turbines are then paralleled to reach the desired power level. The power from the HVDC bus is then fed to the AC grid through a three-phase inverter, avoiding the use of bulky 50/60 Hz transformer inside the nacelle or at the bottom of the wind turbine. The use of a MF transformer instead results in a significant reduction in the overall installed volume/weight, reducing the construction and installation costs of the wind turbine [5]. Special attention must be paid to the level of isolation provided by this transformer, which, in order to be a real replacement for 50/60 Hz transformers, must comply with international standards [6]. Moreover, in the series connection of wind generators presented in Fig. 1-a), the MF transformer must withstand the whole HVDC level. This isolation level is not considered in this work.

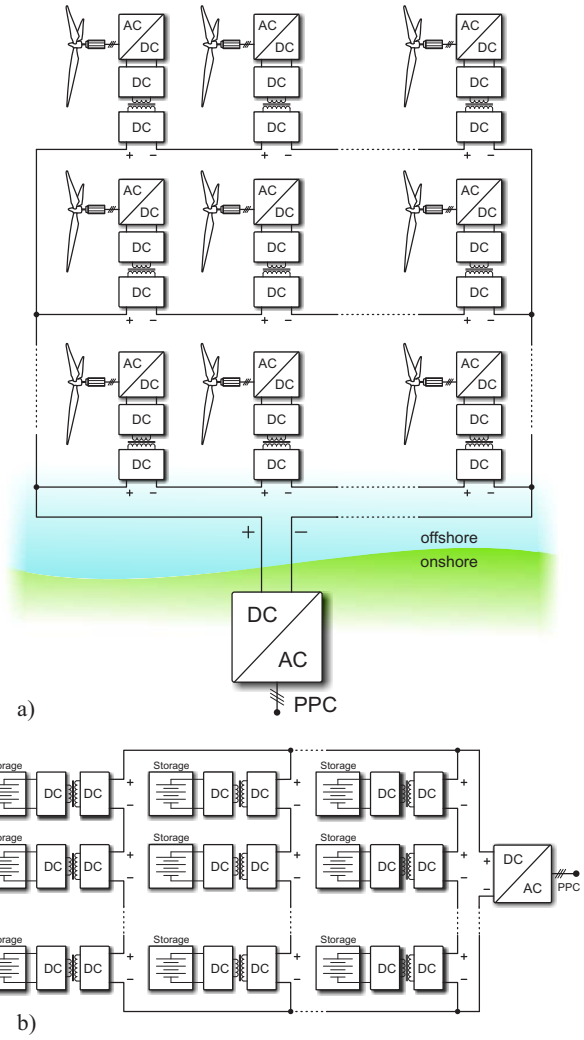

Figure 1: Examples for applications of high-power isolated DC-DC converter in renewable energy generation: a) High power wind farm with HVDC transmission line; b) Energy storage scheme with DC transmission.

In this wind farm layout, each wind turbine's AC-DC converter is connected to a fully rated DC-DC converter. This converter is used to reach the required step-up ratio between the input and output voltages and to provide the required isolation for the wind turbine, given the series connection at the output side. Moreover, by using this DC-DC converter, higher dynamic control is achieved over the power flow.

On the other hand, one drawback of renewable energy sources is their susceptibility to energy fluctuations which, if not properly

TABLE I: Specifications for the isolated, bidirectional DC-DC converter.

Parameter	Value
Power P	1 MW
Switching frequency f_s=1/T_s	20 kHz
Port 1 voltage (high voltage side) V_{HV}	12 kV
Port 2 voltage (low voltage side) V_{LV}	1.2 kV
Isolation (without output series connection)	100 kVDC

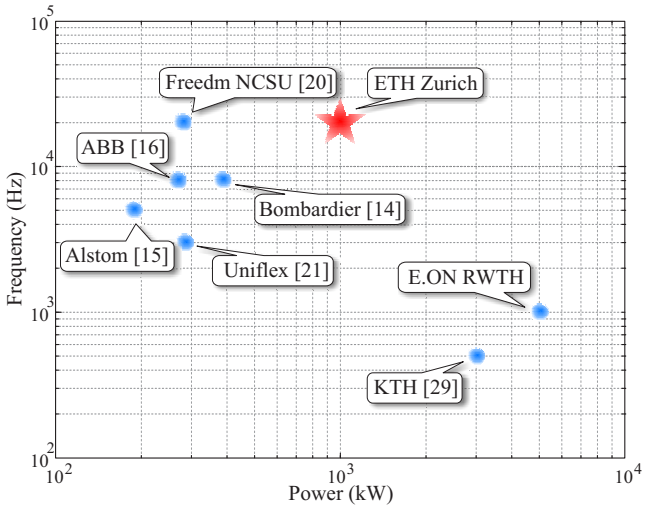

Figure 2: Frequency v/s Power map with different high-power DC-DC converter research efforts.

treated, could lead to instabilities in the power grid or variations in the mains frequency. To overcome these problems, energy storage systems are utilized to store energy during periods of generation surplus and to deliver it during generation sags [7, 8]. Other energy storage systems are meant to provide leveling in the power generation during peak loading, allowing the generators to operate smoothly and closer to their optimum conditions. In both cases, a high-power bidirectional DC-DC converter with high step-up ratio is required to interface with the distribution grid. For larger energy storage schemes, storage systems with their isolated DC-DC converters can be series connected to reach a medium DC voltage level, while the power is reached through parallel connection of grouped storage systems (cf. Fig. 1-b)).

The key enabling technology for these applications is a high-power/high-voltage bidirectional, isolated DC-DC converter. As a consequence, a DC-DC converter with the specifications from Table I is designed. In Fig. 2, a frequency v/s power graph shows the research groups working on DC-DC converters with similar specifications as the ones proposed in this work. As can be seen, several research efforts are addressing the high-power/high-frequency DC-DC converter topic, as it is a key element within future power transmission/distribution grids. Remarkable is also the work performed in [9], where Silicon-Carbide is presented as enabling technology for future converters with powers in the MW range and frequencies in the MHz range.

In this paper, the main research areas that must be addressed to fulfill these requirements are presented. **Section II** presents the High-Voltage (HV) switch options and discusses their performance where the requirements for the topology and modulation of the converter are identified. In order to fulfill these requirements, **Section III** discusses the possibilities for topologies and modulation schemes which are attractive for the application. Three MF transformer concepts are designed in **Section IV** using the calculated voltage and current waveforms.

II. High-Voltage Side Switch

Topologies which allow soft switching conditions (Zero Voltage Switching (ZVS) or ZCS) for semiconductor devices are highly desirable for this application given the selected switching frequency f_s and power rate P (cf. Table I). Additionally, the requirement for bidirectional power flow reduces the possibilities of converter topologies. As a consequence, two converters which allow bidirectional power flow, ZVS and ZCS under certain conditions are considered: The Dual Active Bridge (DAB) and the Series Resonant Converter (SRC). In both cases, the inductive turn-off of the devices represents the most critical processes within the converter operation.

On the other hand, semiconductor switches with high-voltage blocking capability (ranging from 3.3 kV to 6.5 kV) are expected to generate a large share of the converter losses due to their typically slow switching behavior. For that reason, the switching performance of two 4.5 kV IGBT switches is investigated in this section with focus on their turn-off behavior.

An attractive future solution would consider Silicon Carbide (SiC) switches in the HV side. As an example, 6.5 kV SiC JFETs from SiCED are available for testing. By connecting three of these switches in cascode configuration [10], a total blocking voltage capability of 19.5 kV is possible while keeping the high-speed switching behavior of SiC devices in addition to a simple switch control given by a single gate terminal. However, with the presently available 6.5 kV SiC JFETs, only currents in the 5-6 A range could be carried by the switch and therefore this technology is not further considered in this paper.

The 4.5 kV IGBTs switching measurements are used to estimate the losses in the system considering a DAB with trapezoidal modulation, which allows ZVS on the HV IGBTs. Using this estimation, conclusions on the requirements from the topology and modulation point of view will be drawn.

A. 4.5 kV Powerex IGBT

The 4.5 kV Powerex IGBT represents an attractive solution from the packaging point of view, since its gate connection enables fast turn-on behaviors. The testbench depicted in Fig. 3 was built to test the switching performance of this device. Here, two QIS4506002 Powerex switches are connected in series to build a half-bridge. The upper switch is then connected to the load used to test the switch performance.

A turn-off process at 900 V and 600 A is shown in Fig. 5-a). A considerable tail current can be seen here, which causes a large amount of losses (E_{off}=1.51 J) during each turn-off process. An additional test was performed with a 40 nF purely capacitive snubber, where the dissipated turn-off energy reaches in this case E_{off}=0.75 J. In both cases, the large amount of dissipated energy makes this switch unattractive for a 20 kHz operation.

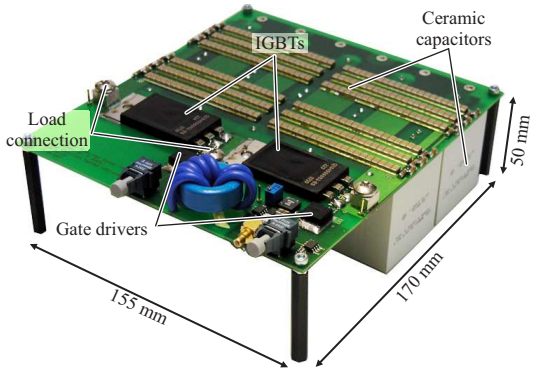

Figure 3: 4.5kV Powerex IGBT Testbench.

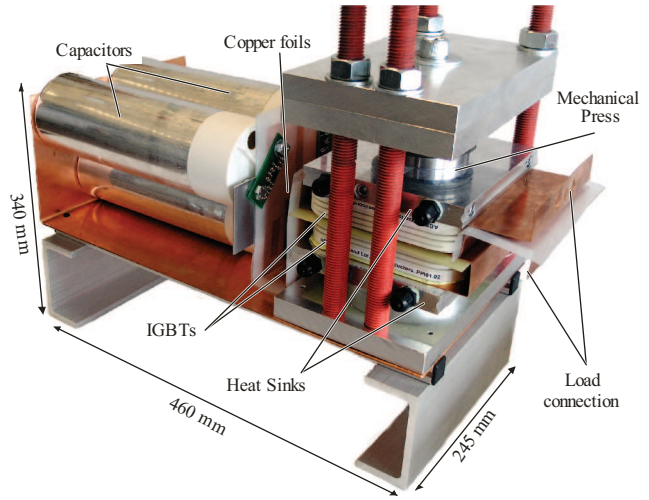

Figure 4: 4.5 kV Press-Pack IGBT Testbench.

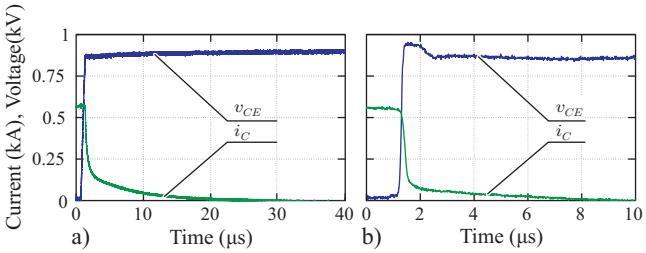

Figure 5: Collector-emitter voltage and collector current of 4.5 kV IGBTs during turn-off behavior: a) Powerex IGBT; b) Press-Pack IGBT.

B. 4.5 kV Press-Pack IGBT

Originally designed for pulsed power and industrial traction applications, the Press-Pack IGBT features 4.5 kV blocking voltage and rated currents in the kA range [11]. The construction of this device is based on single semiconductor chips, which can be either IGBTs or diodes. Several chips are placed on a collector baseplate and the connection to the emitter is then made through special spring contacts designed for equal pressure/current distribution among the chips.

The testbench displayed in Fig. 4 was built to test the performance of this switch. This testbench comprises a capacitor bank which is connected to the IGBT half bridge through coplanar copper foils. Special water-cooled heat sinks are placed over each collector plate to cool the IGBTs. Aluminium plates are then placed above and beneath the setup which are mechanically pressed up to 3 Tons, allowing an even current distribution.

A turn-off process of this switch at 900 V and 600 A is presented in Fig. 5-b). This device presents a better performance on the switching behavior (E_{off}=0.82 J), with a considerably shorter tailing process in comparison to the Powerex device.

C. Efficiency estimation based on DAB converter

In order to quantify the performance of each of these IGBTs, efficiency calculations based on a purely trapezoidal modulation using a DAB converter [12] are now performed. For the LV side switches, the losses were calculated as shown in Section III with the SiC JFET solution. In the case of the transformer, the calculated losses correspond to the matrix transformer discussed in Section IV.

The switching losses considering the powerex IGBT reach 40.3 kW, which correspond to 76.6 % of the overall losses. Similar values are found for the press-pack solution, with switching losses up to 22 kW, corresponding to 64.1 % of the overall converter losses (cf. Fig 8-a)). This high switching losses must be reduced by modifying the converter topology and its modulation scheme. As a consequence, two topologies which allow a ZCS on the HV side are discussed in the following section along with their respective modulation schemes.

III. Topology and Modulation

The two studied topologies that can enable a ZCS in the HV side (HV-ZCS) of the converter are: Dual Active Bridge with triangular modulation and the Series Resonant Converter (SRC) with constant frequency modulation. A $\pm 5\%$ operating range is imposed over the HV and LV levels in order to reach higher robustness. Full power is transferred within these range. The operation principles of each of these converters under HV-ZCS operation will be now discussed.

A. Dual Active Bridge With Triangular Modulation

The DAB is displayed in Fig. 6-a) and it consists of two fullbridge converters each connected to one side of the MF transformer. An inductor ($L_{st,D}$ in Fig 6-a)), which is used as energy transfer component, is placed in series with the transformer, or alternatively, the leakage inductance of the transformer can be used. The operation of this converter under HV-ZCS has been reported previously [13] and is described, according to Fig.6-c), by the following piecewise sequence valid for power transfer from the LV to the HV side:

- Interval *I*: The HV and the LV side bridges apply full positive voltage to the HV and LV windings of the transformer. The difference $V_{LV} - V_{HV}/n_D$ is applied to inductor $L_{st,D}$. If the turns ratio n_D is different to V_{HV}/V_{LV}, then the current $i_{L,D}(t)$ through the transformer rises linearly with slope given by $(V_{LV} - V_{HV}/n_D)/L_{st,D}$. The length of this interval is given by the duty cycle $D_{2,D}$.
- Interval *II*: The LV side bridge switches the voltage $v_{LV}(t)$ to zero, whereas turn-off losses are generated the LV side. The voltage applied to the inductor is now $-V_{LV}/n_D$ and therefore current $i_{L,D}(t)$ decreases with slope $-V_{HV}/n_D/L_{st,D}$. As soon as current $i_{L,D}(t)$ reaches zero, the HV side bridge switches and applies zero voltage to the HV side of the transformer. As the switched current at this point is zero, the turn-off loses are ideally zero. The length of this interval is given by the duty cycle $D_{1,D}$.
- Interval *III*: As approximately no voltage is applied to the inductor $L_{st,D}$, the current through the transformer stays at zero until the second half cycle takes place and the analogous process is repeated. The length of this interval must be adjusted to enable recombination or swap-out of all carriers in the HV IGBT before the next switching cycle begins. This safety margin time is named $t_{SM,D}$.

Using Fig. 6-c), the following equations that describe the behavior of the transformer current $i_{L,D}(t)$ during the first half switching cycle are calculated.

$$i_{L,D}(t) = I_{L0,D} + \frac{v_{E,D}(t)}{L_{st,D}} \cdot t \tag{1}$$

$$v_{E,D}(t) = \begin{cases} V_{LV} - V_{HV}/n_D & : 0 < t \leq D_{2,D}T_s \\ -V_{HV}/n_D & : D_{2,D}T_s < t \leq D_{1,D}T_s \\ 0 & : D_{1,D}T_s < t \leq T_s/2 \end{cases} \tag{2}$$

The initial condition $I_{L0,D}$ is calculated in each switching interval in order to have a continuous current waveform, whereas the initial condition $i_{L,D}(0)$ at interval *I* is calculated to meet with (3).

$$i_{L,D}(0) = -i_{L,D}(T_s/2) \tag{3}$$

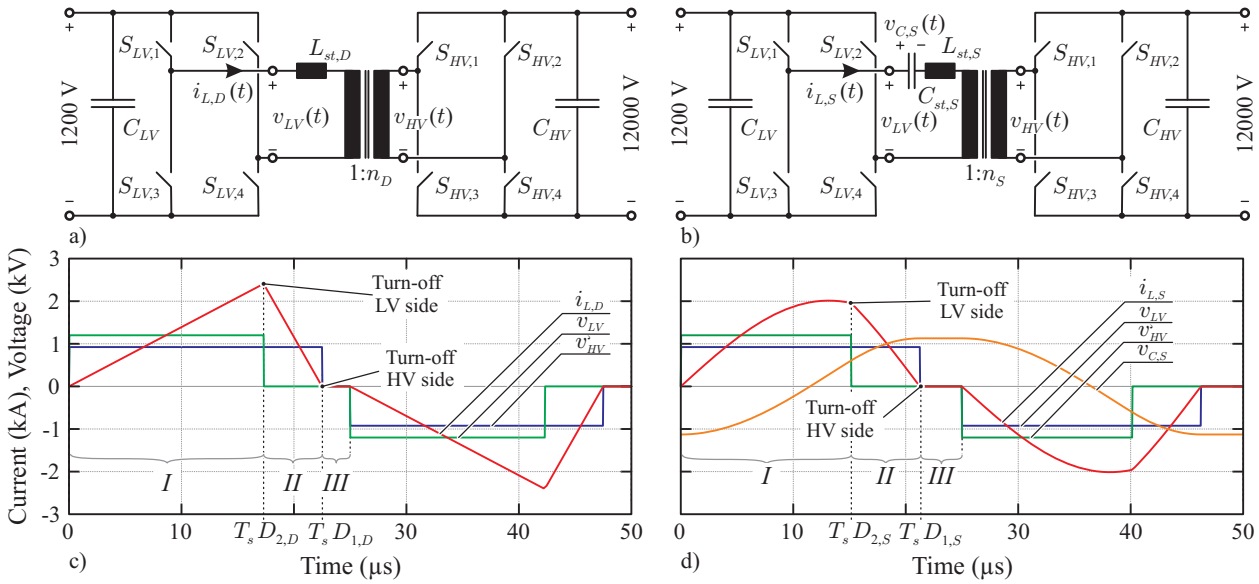

Figure 6: HV side Zero Current Switching bidirectional topologies and modulations: a) Dual Active Bridge; b) Series Resonant Converter; c) DAB triangular modulation with n_D=13 and $L_{st,D}$=2 µH at 1 MW transferred power.; d) SRC constant frequency modulation with n_D=13, $L_{st,D}$=5.85 µH, $C_{st,D}$=12 µF at 1 MW transferred power.

In order to achieve HV-ZCS, the constraint $i_{L,D}(0)$=0 must be fulfilled, which gives a relation between $D_{1,D}$ and $D_{2,D}$ described by (4). The duty cycle $D_{1,D}$ must be adjusted to transfer the required power, thus for a power P_D, the required $D_{1,D}$ is given by (5).

$$D_{2,D} = \frac{V_{HV} \cdot D_{1,D}}{n_D \cdot V_{LV}} \tag{4}$$

$$D_{1,D} = \frac{n_D \sqrt{T_s(V_{LV} \cdot n_D - V_{HV}) L_{st,D} n_D V_{LV} P_D}}{T_s(V_{LV} \cdot n_D - V_{HV}) V_{HV}} \tag{5}$$

In this modulation scheme, the turns ratio must be different to the input output voltage ratio V_{HV}/V_{LV}, otherwise no power is transferred. Additionally, to achieve HV-ZCS, the turns ratio must be higher than the input output voltage ratio V_{HV}/V_{LV}. Therefore the limitation on the turns ratio is given by:

$$n_D > \frac{V_{HV}}{V_{LV}} \tag{6}$$

The series inductance $L_{st,D}$ is designed to have a certain safety margin time $t_{SM,D}$ in worst case between the turn-off of the HV switch and the start of the next switching cycle. This in turn gives a relation between the turns ratio n_D and the series inductance $L_{st,D}$.

With this description, the turns ratio n_D and the safety margin $t_{SM,D}$ are left as design parameters. The turned-off currents, RMS and average currents in the switches are calculated for a given transferred power P_D. Thereafter, an optimized design can be reached by following the optimization process shown in Fig. 7.

B. Series Resonant Converter with Constant Frequency Modulation

The SRC converter depicted in Fig.6-b), represents an attractive alternative for the HV-ZCS current modulation, which led to several high power DC-DC converter research efforts [14–16]. This converter consists of two full bridges interfaced by a transformer with a series resonant tank composed of an inductor $L_{st,S}$ and a capacitor $C_{st,S}$. Piecewise sinusoidal current waveforms are obtained through the transformer with this resonant tank.

As has been reported in [17], the power transfer of this converter can be controlled by adjusting the switching frequency with a 50 % duty cycle in both fullbridges. However, given the desired HV-ZCS behavior and the operating ranges of the system, this operating mode is not suitable for the following reasons:

- Over-resonant frequency: In this operating mode, the current $i_{L,S}(t)$ has always a phase difference with respect to the driving voltage. This implies that, when the power is transferred from the HV to the LV side, the HV side switches will turn-off the transformer current and thus HV-ZCS would not be achievable.
- Under-resonant frequency: In this operating mode, only buck operation is achievable by reducing the switching frequency starting from resonant frequency. This means that the voltage ranges can not be covered once a turns ratio n_S is selected.

Constant frequency operation of the SRC converter was treated in [18] for several state trajectories. Of special interest is the trajectory that enables a HV-ZCS behavior, which is presented in Fig.6-d) and described by the following piecewise intervals:

- Interval *I*: The HV and the LV side bridges apply full positive voltage to the HV and LV windings of the transformer. The difference $V_{LV} - V_{HV}/n_S$ is applied to the resonant tank. The current $i_{L,S}(t)$ through the transformer rises with a sinusoidal waveform and consequently the resonant capacitor voltage $v_{C,S}(t)$ varies sinusoidally (cf. *I* Fig.6-d)). The length of this interval is given by the duty cycle $D_{2,S}$.
- Interval *II*: The LV side bridge switches the voltage $v_{LV}(t)$ to zero, whereas turn-off losses are generated the LV side. The voltage applied to the tank is now $-V_{LV}/n_S$ and therefore the current decreases. As soon as current $i_{L,S}(t)$ reaches zero,

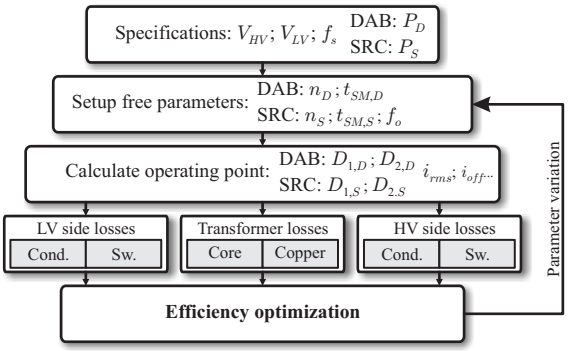

Figure 7: Flow-chart of converter's optimization process.

the HV side bridge switches and applies zero voltage to the HV side of the transformer. As the switched current at this point is zero, the turn-off loses are negligible. The length of this interval is given by the duty cycle $D_{1,S}$.

- Interval *III*: If capacitor voltage $v_{C,S}(t)$ is lower than the low side voltage V_{LV} and the reflected high side voltage V_{HV}/n, then the corresponding diodes are in blocking state and therefore the current through the transformer stays at zero until the next half switching period begins. The resonant frequency f_0 is must be adjusted to enable recombination or swap-out of all carriers in the HV IGBT before the next switching cycle begins. This safety margin time is named $t_{SM,S}$.

Considering the time intervals in Fig.6-d), the current $i_{L,S}(t)$ and the voltage $v_{C,S}(t)$ are described by the following set of equations [18] for the first half switching period:

$$i_{L,S}(t) = -\frac{(V_{C0,S} - v_{E,S}(t))}{Z_0}\sin(\omega_0 t) + I_{L0,S}\cdot\cos(\omega_0 t) \quad (7)$$

$$v_{C,S}(t) = (V_{C0,S} - v_{E,S}(t))\cdot\cos(\omega_0 t) \quad (8)$$

$$+ I_{L0,S}Z_0\cdot\sin(\omega_0 t) + v_{E,S}(t) \quad (9)$$

$$\omega_0 = \sqrt{\frac{1}{L_{st,S}C_{st,S}}} = 2\pi f_0 \quad (10)$$

$$Z_0 = \sqrt{\frac{L_{st,S}}{C_{st,S}}} \quad (11)$$

$$v_{E,S}(t) = \begin{cases} V_{LV} - V_{HV}/n & : 0 < t \le D_{2,S}T_s \\ -V_{HV}/n_S & : D_{2,S}T_s < t \le D_{1,S}T_s \\ 0 & : D_{1,S}T_s < t \le T_s/2 \end{cases} \quad (12)$$

The initial conditions $V_{C0,S}$ and $I_{L0,S}$ are calculated in each switching interval in order to have a continuous voltage/current waveforms, whereas the initial conditions $i_{L,S}(0)$ and $v_{C,S}(0)$ at interval *I* are calculated to meet with (13) and (14) respectively.

$$i_{L,S}(0) = -i_{L,S}(T_s/2) \quad (13)$$

$$v_{C,S}(0) = -v_C(T_s/2) \quad (14)$$

The aim is to achieve HV-ZCS, which is equivalent to forcing $i_{L,S}(0)$=0 and solving for $D_{2,S}$, thus finding the relation between $D_{1,S}$ and $D_{2,S}$ given by (15). The duty-cycle $D_{1,S}$ is then adjusted to transfer a power P_S through the converter as described by (19).

$$D_{2,S} = -\tan^{-1}\left(\frac{F_1 n_S v_{C,S}(0)}{F_2(n_S V_{LV} - n_S v_{C,S}(0) - n_S V_{HV}) - n_S V_{LV}} - \frac{n_S V_{LV} + V_{HV}}{F_2(n_S V_{LV} - n_S v_{C,S}(0) - n_S V_{HV}) - n_S V_{LV}}\right)\frac{f_s}{\omega_0} \quad (15)$$

$$F_1 = \sin(\omega_0 D_{1,S} T_s) \quad (16)$$

$$F_2 = \cos(\omega_0 D_{1,S} T_s) \quad (17)$$

$$v_{C,S}(0) = \frac{V_{LV}(F_2 V_{LV} n_S - F_2 V_{HV} - V_{LV} n_S)}{2V_{HV} + F_2 V_{LV} n_S - V_{LV} n_S} \quad (18)$$

$$D_{1,S} = \cos^{-1}\left(\frac{4 f_s (V_{LV}^2 V_{HV} - V_{LV} V_{HV}^2)}{V_{LV}(4 f_s V_{HV} n_S V_{LV} - 4V_{HV}^2 f_s + P_S Z_0 \omega_0 n_S^2)} + \frac{P_S \cdot Z_0 \omega_0 (n_S^2 V_{LV} - 2 n_S V_{HV})}{V_{LV}(4 f_s V_{HV} n_S V_{LV} - 4V_{HV}^2 f_s + P_S Z_0 \omega_0 n_S^2)}\right)\frac{f_s}{\omega_0} \quad (19)$$

The same constraint as with the DAB stands for the turns ratio n_S, (cf. (6)). The resonant frequency f_0 is chosen to have a defined $t_{SM,S}$ in worst-case operation. This frequency is usually in the range f_0=0.8..0.9f_s [13]. The series capacitor $C_{st,S}$ should be large enough to avoid conduction of the diodes during interval *III*.

With (7)-(18) the operation of the converter is described, leaving n_S, $t_{SM,S}$ and $C_{st,S}$ as design parameters. The turned-off currents, RMS and average currents in the switches are calculated for a given transferred power P_S. Thereafter, an optimized design can be reached by following the optimization process shown in Fig. 7.

TABLE II: Design parameters for the DAB and the SRC topologies.

Parameter	DAB	SRC
Turns ratio	n_D=13	n_S=13
Safe M. time	$t_{SM,D}$=2.5 µs	$t_{SM,S}$=2.5 µs
Series inductance	$L_{st,D}$=2 µH	$L_{st,S}$=5.85 µH
Series capacitor	-	$C_{st,S}$=12 µF
Resonant frequency	-	f_0=19 kHz

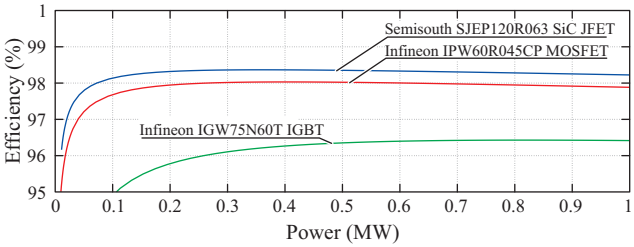

Figure 9: Calculated efficiencies for DAB with triangular modulation using different LV-side switch technologies.

C. *Efficiency comparison for different LV side switches*

With the aforementioned modulation schemes, the desired HV-ZCS is achieved, where all the switching processes are performed by the LV side switches. In this voltage range, mature technologies with high switching performances can be found. In this section, the efficiencies of both studied topologies considering the following switch technologies are investigated:

- 600 V IGBT: Infineon IGW75N60T
- 600 V MOSFET: Infineon CoolMOS IPW60R045CP
- 1200 V SiC JFET: Semisouth SJEP120R063

These devices are single switches which require to be paralleled in order to reach the current driving capability. A total of 60 switches are paralleled to build one of the power switching device, which will be then fitted into one power module. In the case of IGBTs and MOSFETS, the blocking capability is reached through a series connection of 3 groups of paralleled devices, whereas in case of the SiC JFETs, only 2 series connected groups of devices are required. For the HV side, each of the switches is built using 4 series connected Press-Pack IGBTs.

The safe blocking voltage distribution in the series connected devices in both LV and HV sides can be achieved by addition of passive components or by using a multilevel (ML) construction [19–21]. When considering a Neutral Point Clamped (NPC) ML converter in two level operation, no additional losses are generated in the clamping diodes [22] and therefore the losses calculations can be performed considering an ideal series connection of switches. Two level operation is considered at full transferred power whereas at partial load, the staircase-type voltage of the ML topology could be used to increase the soft-switching range. This last case is not treated in this paper.

The losses in the LV side switches are calculated using datasheet information whereas for the HV side switches the measured output characteristic is used. The transformer losses are included in the efficiency calculations considering the matrix transformer construction presented in Section IV, which represents a worst case in terms of losses. In the case of the SRC converter, the losses in the series capacitor are included in the transformer losses.

The parameters used to perform the efficiency comparison between both converters are shown in Table II.

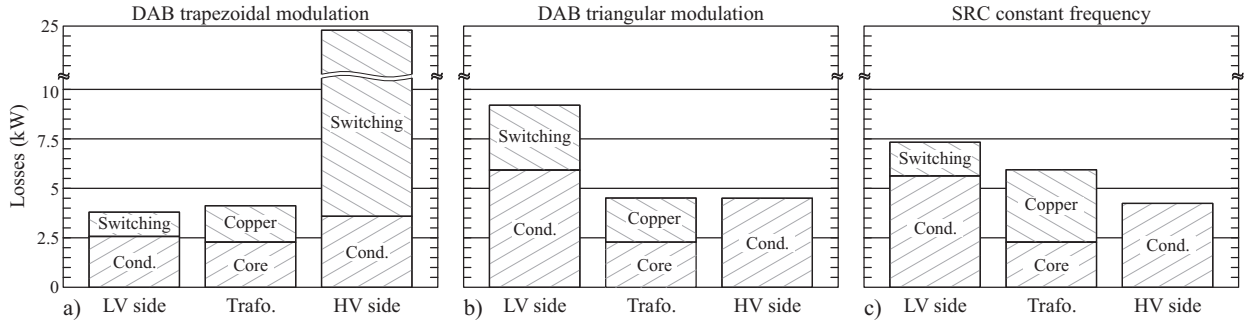

Figure 8: Loss distribution at power $P = 1\,\mathrm{MW}$ for the SiC JFET LV switch solution and the matrix transformer design: a) DAB with trapezoidal modulation; b) DAB with triangular modulation; c) SRC with constant frequency.

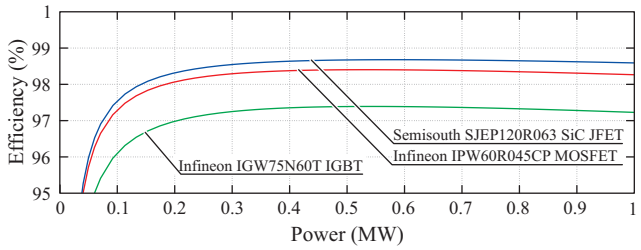

Figure 10: Calculated efficiencies for SRC with constant frequency modulation using different LV-side switch technologies.

Figs. 9 and 10 show the calculated average efficiencies for both topologies as function of the transferred power for the different LV switch technologies. As can be seen, a considerable improvement in efficiency is achieved in comparison with a DAB-trapezoidal modulation in all cases. The SiC JFET solution appears specially attractive, with efficiencies over 98 % for both topologies. The best performance is achieved with the SiC JFET solution using the SRC converter. Here a 98.6 % efficiency is reached at nominal power. This is mainly due to the lower switched-off currents in relation to the DAB converter, given the resonant operation. However, special attention should be payed to capacitor $C_{st,S}$, which must be able to withstand high voltages and to carry the whole transformer current (cf. Fig. 6-c)).

The loss distribution among the converter components for the studied topologies is presented in Fig. 8 including the DAB with trapezoidal modulation. As can be seen, compared to the trapezoidal modulation, the losses in the HV switches are drastically reduced with the triangular modulation and the SRC constant frequency modulation as ideally no switching losses are generated in these devices . In turn, the switching losses are now taken by the LV side switches, which posses better switching performances and, despite the high switched-off currents, enable high efficiencies of the converter (cf. Fig. 9 and 10).

A further step in the topology and modulation is to perform an optimal design of all the components for both the DAB and the SRC topologies in order to choose the most attractive solution for application in hand.

IV. Medium Frequency Transformer

The MF transformer is used mainly for two purposes: step-up/down the voltage levels and to provide the required isolation between HV and LV sides (cf. Table I). This last feature is particularly critical as it is closely linked to the losses and power density of the transformer, as will be shown in the following sections.

The voltage and current waveforms are extracted from the modulation scheme in order to design the transformer. The DAB with triangular modulation is used as reference as it represents a worst case in terms of HF losses. The voltage applied to the transformer,

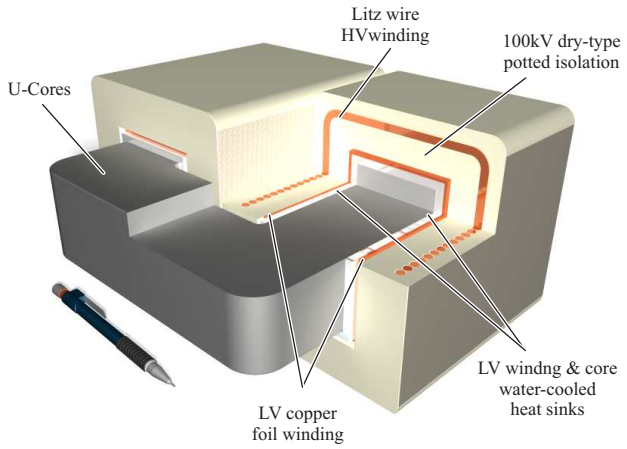

Figure 11: Core-type transformer. Size: 294 mmx284 mmx141 mm. Core losses: 1.26 kW, Copper losses 1.55 kW.

which determines the core cross-section and the number of turns, is assumed as square-shaped with 50 % duty cycle. The core material in all cases is the VITROPERM 500F.

As the transformer is responsible for a large share of the volume and losses of the converter, it is desirable to study different constructions and isolation mechanisms. Moreover, with high power densities, thermal management complexity is increased due to more compact converter constructions. It is therefore desirable to rely on good thermal extraction mechanisms, which would allow to increase the power density of the transformer.

In the following, the design of three different transformer concepts, namely U-core, shell-type and matrix transformer with different isolation mechanisms is presented. For the winding losses, HF skin and proximity effects were included as described in [23] whereas in case of the core losses, non-sinusoidal effects of the applied voltage were included as described in [24]. For each concept, a description of the winding arrangement, the isolation and thermal management is performed and compared. In future, this last topic will be investigated more in detail.

A. U-Core Transformer

The U-Core transformer arrangement is based on a single magnetic core with windings in both legs of the core [25]. A 3D CAD design of the transformer for this applications is presented in Fig. 11.

1) Winding Arrangement: The LV winding is built with two HF-optimized copper foils of 0.3 mm. Each leg of the core has one of these 4-turn LV windings which are then parallel connected. The current distribution between these windings is then actively controlled by the converter. The HV winding is built with a litz wire of 840 strands of 0.1 mm each. Two windings composed of

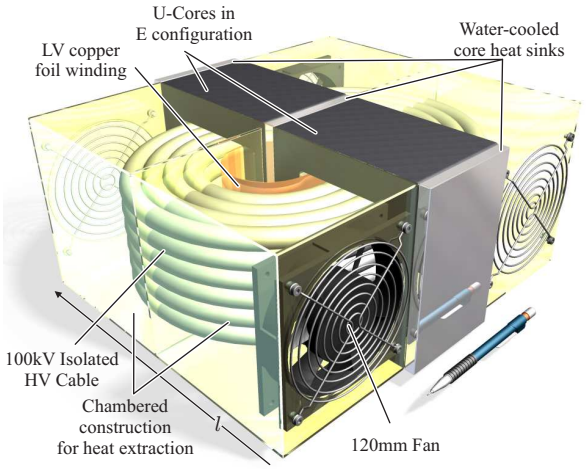

Figure 12: Shell-type transformer. Size: 358 mmx324 mmx163 mm. Core losses: 1.83 kW, Copper losses 1.93 kW.

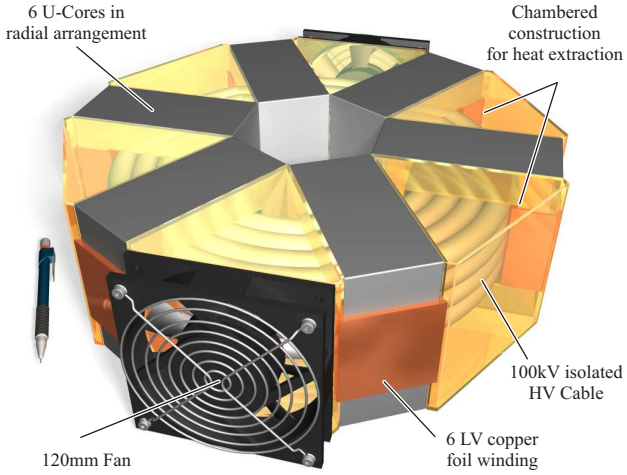

Figure 13: Matrix transformer. Size: Outer Diam.= 396 mm, Height=120 mm. Core losses: 2.23 kW, Copper losses 2.28 kW.

26 turns each are wound around the LV windings and then series connected

2) Isolation: The isolation is achieved by placing a 20 mm dry-isolation layer between primary and secondary of the transformer (cf. Fig. 11). This distance is required to integrate the series inductance within the transformer's leakage inductance. A 300 kV isolation is achieved using the Micares© [26] material with this isolation layer. This dry-type isolation enables a compact transformer construction with a total volume of 4.3 liter. Moreover, as the required winding window is reduced, the size of the core is also reduced, decreasing the core losses. The use of a litz-wire optimized for HF operation further reduces the transformer losses which are 3.5 kW at 1 MW.

3) Thermal Management: To extract the losses of the LV winding and core, water-cooled heat sinks are placed, on one side against the core surface and on the other side on the LV winding surface (cf. Fig. 11). For the HV winding, water-cooled heat sinks are placed on the outer face of the cast isolation where the heat is transferred through the outer isolation layer [27].

Another proposed heat extraction mechanism consists of using a braided hollow copper conductor with an internal plastic hose carrying water. This water-cooled cable was proposed in [28] for a battery charging system.

B. Shell-Type Transformer

This transformer construction consists of two pairs of U cores arranged in "E-core" configuration as depicted in Fig. 12 and reported in [25, 29].

1) Winding arrangement: The LV winding is built using an HF-optimized 0.5mm thick copper foil wound around the middle leg formed by the two pairs of U cores. The HV winding is then placed around the LV winding using a 133 strand HV cable [30]. The maximum bending radius of this cable determines the length l of the transformer, as can be seen in Fig. 12.

2) Isolation: The HV cable used for the HV winding is able to withstand a 100 kVDC isolation using a silicon-based material [30]. The use of this isolation mechanism significantly reduces the complexity of the transformer construction in relation to the U-core transformer, as no custom made parts are required to reach the isolation level.

It should be noted that the 100 kVDC isolation must be achieved between LV and HV windings. However, by using a HV cable, there exists a double isolation level between each HV turn. This unavoidable issue increases the core and winding sizes drastically, increasing the volume of the transformer to 11.9 liter. With these larger core and winding sizes, the losses in the transformer are higher, which added to the not HF-optimized litz HV conductor, reach 3.76 kW in this case at full power.

3) Thermal Management: Water-cooled heat-sinks as depicted in Fig. 13 are placed between the core and the windings for the heat extraction of the core and LV windings. Additional heat sinks are placed in the outer face of the core to exact the core heat. Two chambers are created by an additional enclosure to create independent ventilation ducts through which respective 120 mm fans blow to cool the HV winding. The distance between each HV winding turn must be adjusted to enable the required heat extraction.

Another shell-type transformer was designed considering a litz wire for the HV side winding with a potted isolation as with the U-core transformer. The volume is reduced to 3.5 liter and the losses to 3.37 kW with this isolation type.

C. Matrix Transformer

An attractive solution is represented by matrix transformer arrangement [31]. Here several magnetic cores are interwired with series/parallel conductors, reaching the desired HV to LV transformation ratio []. A 3D CAD drawing of the designed matrix transformer is shown in Fig. 13.

1) Winding Arrangement: As shown in Fig. 13, the designed matrix transformer consists of 6 magnetic core units, each with a LV winding consisting of 8 turns of a HF-optimized 0.3 mm copper foil. Through all 6 cores, 16 turns of a HV cable [30] are wound (cf. Fig. 13), where each core unit has a 1:2 turns ratio reaching a total turns ratio of $A_{LV}/A_{HV} \cdot 1/2$=1:12 for the whole transformer.

The main advantage of this transformer construction is the requirement of less HV cable turns in comparison to the core and shell-type transformers, significantly reducing the transformer construction complexity. Also, by using separated magnetic core units, a magnetic paralleling of semiconductors is possible, enabling a better current distribution among the devices [32].

2) Isolation: The HV cable reaches an isolation level of 100 kVDC using a silicon-based isolation material [30]. As with the shell-type transformer with HV cable, the unavoidable distance between each HV conductor significantly affects the overall volume of the system, reaching a total volume of 11 liter. By this same fact, together with the not HF-optimized HV cable, the transformer losses are affected, reaching 4.5 kW at nominal power.

3) Thermal Management: The thermal management of the core and LV windings has a reduced complexity since more area is

TABLE III: Performance of the different transformer concepts at 1 MW transferred power.

Type	Losses (Core/Copper)	Volume	Isolation
Core-Type	2.81 kW (1.26 kW/1.55 kW)	4.3 liter	Potted
Shell-Type 1	3.76 kW (1.83 kW/1.93 kW)	11.9 liter	Cable
Shell-Type 2	3.37 kW (950 W/2.42 kW)	3.5 liter	Potted
Matrix	4.51 kW (2.23 kW/2.28 kW)	11 liter	Cable

available for heat extraction, enabling the use of water-cooled heat-sinks for each magnetic core.

A chamber construction as displayed in Fig. 13 can be used for the HV winding. Here, special enclosures are used to create a ventilation path. On each side of the transformer, 120 mm fans are used to blow air through the HV cable, extracting the heat from this component.

Table III summarizes the design of each of the presented transformer concepts. As discussed in each of the transformers' description, the isolation concept has a great impact over the overall volume and losses of the transformer. As can be seen, for similar power losses, the transformers with HV cable isolation present a volume $\sim$300 % larger than the potted-isolated concepts. However, the advantage coming with this isolation solution is a much easier transformer construction, which avoids manufacturing custom made potted windings for the HV side.

V. Conclusions

A 1 MW, 20 kHz, bidirectional, isolated DC-DC converter for 1.2 kV and 12 kV voltage levels is proposed for renewable energy applications.

Given the slow switching behavior of the HV switches currently available, high switching losses are generated when turning-off inductive currents. To reduce these switching losses, bidirectional topologies with ZCS capabilities, namely the DAB with triangular modulation and SRC with constant frequency operation, are considered. When calculating the overall system losses for different LV switch technologies, a better performance regarding efficiency was found with the SRC converter. Both HV-ZCS topologies achieve a considerable reduction in the overall losses compared to a traditional DAB with trapezoidal modulation, reaching an efficiency of 98.6 % in the best case.

Three different transformer concepts were revised. Here, a clear trade-off between mechanical construction complexity and power density was observed. Total losses of 2.81 kW and a volume of 4.3 liter are reached in best case with the U-core transformer and a potted isolation. In case of the matrix concept, by using a HV cable for isolation purposes, total losses of 4.51 kW are reached while the volume is increased to 11 liter.

References

[1] C. Aubrey, "Energy Revolution, A Sustainable Global Energy Outlook," European Renewable Energy Council, Tech. Rep., 2009.

[2] C. Meyer, "Key Components for Future Offshore DC Grids," Ph.D. dissertation, RWTH Aachen, 2007.

[3] J. L. M. Iñigo Martínez de Alegría, "Transmission alternatives for offshore electrical power," *Renewable and Sustainable Energy Reviews*, vol. Volume 13, Issue 5, pp. 1027–1038, June 2009.

[4] S. Lundberg, "Wind Farm Configuration and Energy Efficiency Studies - Series DC versus AC Layouts," Ph.D. dissertation, Department of Energy and Environment - Chalmers University of Technology, 2006.

[5] ECPE, "Research Challenges and Visions on Megawatt Power Electronics and Smart Grids," in *ECPE proceedings*, 2009.

[6] *IEEE Standard General Requirements for Dry-Type Distribution and Power Transformers Including Those With Solid Cast and/or Resin-Encapsulated Windings*, IEEE Std.

[7] M. Gibescu, W. Kling, B. Ummels, E. Pelgrum, and R. van Offeren, "Case study for the integration of 12GW wind power in the dutch power system by 2020," in *Integration of Wide-Scale Renewable Resources Into the Power Delivery System, 2009 CIGRE/IEEE PES Joint Symposium*, july 2009.

[8] P. Pinson, G. Papaefthymiou, B. Klockl, and J. Verboomen, "Dynamic sizing of energy storage for hedging wind power forecast uncertainty," in *Power Energy Society General Meeting, 2009. PES '09. IEEE*, july 2009, pp. 1 –8.

[9] I. Takahashi, "SiC power converters and their applications in near future," *IEEJ, Industry Applications Society*, vol. 1, pp. 279 – 284, 2001.

[10] J. Biela, D. Aggeler, D. Bortis, and J. W. Kolar, "5kv/200ns pulsed power switch based on a sic-jfet super cascode," in *Proc. IEEE International Power Modulators and High Voltage Conference the 2008*, 27–31 May 2008, pp. 358–361.

[11] S. Eicher, M. Rahimo, E. Tsyplakov, D. Schneider, A. Kopta, U. Schlapbach, and E. Carroll, "4.5kV press pack IGBT designed for ruggedness and reliability," in *39th IAS Annual Meeting Industry Applications Conference Conference Record of the 2004 IEEE*, vol. 3, 3–7 Oct. 2004, pp. 1534–1539.

[12] R. W. A. A. De Doncker, D. M. Divan, and M. H. Kheraluwala, "A three-phase soft-switched high-power-density DC/DC converter for high-power applications," vol. 27, no. 1, pp. 63–73, Jan.–Feb. 1991.

[13] F. Krismer, J. Biela, and J. Kolar, "A comparative evaluation of isolated bi-directional DC/DC converters with wide input and output voltage range," in *Industry Applications Conference, 2005. Fourtieth IAS Annual Meeting. Conference Record of the 2005*, vol. 1, oct. 2005, pp. 599 – 606 Vol. 1.

[14] M. Steiner and H. Reinold, "Medium frequency topology in railway applications," in *Power Electronics and Applications, 2007 European Conference on*, sept. 2007, pp. 1 –10.

[15] J. Taufiq, "Power Electronics Technologies for Railway Vehicles," in *Power Conversion Conference - Nagoya, 2007. PCC '07*, april 2007, pp. 1388 –1393.

[16] D. Zuber, "Mittelfrequente Resonante DC/DC-Wandler für Traktionsanwendungen," Ph.D. dissertation, ETH Zürich, 2001.

[17] R. Steigerwald, "A comparison of half-bridge resonant converter topologies," *Power Electronics, IEEE Transactions on*, vol. 3, no. 2, pp. 174 –182, apr 1988.

[18] F.-S. Tsai, P. Materu, and F. Lee, "Constant-frequency clamped-mode resonant converters," *Power Electronics, IEEE Transactions on*, vol. 3, no. 4, pp. 460 –473, oct 1988.

[19] D. V. Ghodke, K. Chatterjee, and B. G. Fernandes, "Three-Phase Three Level, Soft Switched, Phase Shifted PWM DC-DC Converter for High Power Applications," vol. 23, no. 3, pp. 1214–1227, May 2008.

[20] L. Yang, T. Zhao, J. Wang, and A. Q. Huang, "Design and Analysis of a 270kW Five-level DC/DC Converter for Solid State Transformer Using 10kV SiC Power Devices," in *Proc. IEEE Power Electronics Specialists Conference PESC 2007*, 17–21 June 2007, pp. 245–251.

[21] [Online]. Available: http://www.eee.nottingham.ac.uk/uniflex/

[22] M. Schweizer, T. Friedli, and J. Kolar, "Comparison and implementation of a 3-level NPC voltage link back-to-back converter with SiC and Si diodes," in *Applied Power Electronics Conference and Exposition (APEC), 2010 Twenty-Fifth Annual IEEE*, feb. 2010, pp. 1527 –1533.

[23] C. Sullivan, "Winding loss calculation with multiple windings, arbitrary waveforms, and two-dimensional field geometry," in *Industry Applications Conference, 1999. Thirty-Fourth IAS Annual Meeting. Conference Record of the 1999 IEEE*, vol. 3, 1999, pp. 2093 –2099 vol.3.

[24] K. Venkatachalam, C. Sullivan, T. Abdallah, and H. Tacca, "Accurate prediction of ferrite core loss with nonsinusoidal waveforms using only steinmetz parameters," in *Computers in Power Electronics, 2002. Proceedings. 2002 IEEE Workshop on*, june 2002, pp. 36 – 41.

[25] T. Kjellqvist, S. Norrga, and S. Ostlund, "Design considerations for a medium frequency transformer in a line side power conversion system," in *Power Electronics Specialists Conference, 2004. PESC 04. 2004 IEEE 35th Annual*, vol. 1, june 2004, pp. 704 – 710 Vol.1.

[26] [Online]. Available: http://www.abb.com/

[27] J. Biela and J. Kolar, "Cooling concepts for high power density magnetic devices," in *Power Conversion Conference - Nagoya, 2007. PCC '07*, april 2007, pp. 1 –8.

[28] C. Conrady, "High Power, High Frequency, Liquid-Cooled Transmission Cable and Charging Systems," U.S. Patent 5 670 860, 1995.

[29] S. Meier, T. Kjellqvist, S. Norrga, and H.-P. Nee, "Design considerations for medium-frequency power transformers in offshore wind farms," in *Power Electronics and Applications EPE*, sept. 2009, pp. 1 –12.

[30] [Online]. Available: www.hivolt.com/

[31] E. Herbert, "High Frequency Matrix Transformer," U.S. Patent 4 845 606, 1989.

[32] D. Bortis, J. Biela, and J. Kolar, "Transient behaviour of solid state modulators with matrix transformers," in *Pulsed Power Conference, 2009. PPC '09. IEEE*, 28 2009-july 2 2009, pp. 1396 –1401.